IEEE Access
Multidisciplinary ⋮ Rapid Review ⋮ Open Access Journal

Received July 28, 2020, accepted August 9, 2020, date of publication August 14, 2020, date of current version August 25, 2020.

Digital Object Identifier 10.1109/ACCESS.2020.3016663

Modeling and Simulation Analysis of Wet Multi-Disk Service Braking System for Heavy Vehicles

YONG YANG[1,3], HAIBAO WANG[1,2], AND GUOFENG XIA[1]

[1]School of Mechanical Engineering, Chongqing Three Gorges University, Chongqing 404100, China
[2]Chongqing Engineering Technology Research Center for Light Alloy and Processing, Chongqing Three Gorges University, Chongqing 404100, China
[3]School of Materials Science and Engineering, University of Science and Technology Beijing (USTB), Beijing, China

Corresponding author: Yong Yang (20140049@sanxiau.edu.cn)

This work was supported by the Chongqing Municipal Education Commission Project of China under Grant KJ1501021.

ABSTRACT A new type of charging valve with electro-hydraulic closed-loop feedback is designed, and a wet multi-disc dual-circuit service brake is built based on AMEsim. The charging and discharging characteristics of the accumulator are studied. The results show that under the condition of a medium-flow constant current source, the dual-circuit accumulator responds quickly, and a single charging can smoothly provide multiple stable discharge output. The response to the pressure output caused by the static structural parameters of the tandem braking valve and the pedal signal is studied. The results show that: the pedal signal can significantly change the brake pressure output, but the preload of the return spring is not apparent; the change of the cross-sectional diameter of the rear axle spool will cause the spool opening lags, and the difference in the spool diameter will cause the spool closing lags. The time response performance of single-axle braking and dual-axle braking is studied. The response from environmental factors such as road adhesion coefficient, slope, load, and brake cool modes to braking distance, braking deceleration, and braking temperature is studied. We establish a parameter ranges of braking safety zone and braking safety comfort zone. This study provides a comparison and reference to the design of a new charging valve and the performance test of the service braking system of heavy vehicles.

INDEX TERMS Charging valve, service brake, system simulation, wet multi-disc, wheel loader.

I. INTRODUCTION

The service braking system for heavy vehicles with pneum-atic braking or full hydraulic braking usually consists of two parts in series: the charging circuit and the brake circuit. The basic principle of braking is that the hydraulic pump in the charging circuit fills the high-pressure accumulator with oil through the charging valve or the supercharger to store pressure energy. When the vehicle requires braking, the hydraulic brake valve pedal is stepped on to make the accu-mulator release the pressure energy, and act on the brake to generate braking. There are two main braking methods for brakes: caliper disc brake and wet multi-disc brake. Compa-red with the caliper disc brake structure, the wet multi-disc brake environment is fully enclosed. It has the characterist-ics of substantial anti-environ-mental pollution, low wear, and a comfortable increase of braking torque. Therefore, the wet multi-disc brake system has become an important research topic for the safety braking heavy vehicles.

From the composition of the brake system, the brake system mainly includes wet multi-disc brakes, brake valves, accumulators, charging valves, pipelines, oil pools, and other auxiliary equipment. Researchers often analyze the causes of mechanical, thermal effects from braking in [1]. Through structural optimization, thermo-elastic theory modeling, numerical simulation in [2]–[4], and experimental comparison in [5]–[7] or other methods to study the thermal mechanism, analyze the relationship between the thermo-flow field and the corresponding physical quantity changes. In addition to brakes, the brake valve and the charging valve are also concerned by researchers. By changing the static structural parameters of the brake valve and charging valve in [8]–[13], scholars have studied the static and dynamic output response of the brake system.

From the perspective of local improvement or algorithm control of the brake system, in terms of pump or valve control, the critical application of the electro-hydraulic brake

The associate editor coordinating the review of this manuscript and approving it for publication was Tao Wang.

system (EHB) in the vehicle is summarized in [14]. EHB has the advantages of stable and fast hydraulic pressure control, natural to realize regenerative braking, and accurate control through an algorithm. From the perspective of control algorithms, Sabanovic *et al.* [15] used a friction coefficient based on deep neural networks to estimate and recognize the type of road surface, Cao *et al.* [16] studied the lane detection algorithm of intelligent vehicles under complex road conditions. Moaveni and Barkhordari [17] modeled and recognized the hydraulic anti-skid braking system, and designed a control algorithm driven by inform-ation on the road conditions (dry, wet, etc.). Castillo *et al.* [18] used an estimation algorithm based on Kalman filter to obtain the adhesion between the wheel and the road surface and the speed of the vehicle, and developed a new control block to control the braking pressure more rapidly and more accurately. Sakai *et al.* [19] proposed a dynamic driving / braking force distribution algorithm for independent four-wheel drive. Jin *et al.* [20] studied the low-speed control of downhill vehicles based on the Fuzzy-PID control algorithm.

In terms of environmental factors affecting braking performance, Tang *et al.* [4] studied the influence of brake pads on vibration and noise under wet and dry conditions. Klein-Paste [21] studied the braking friction under the terms of dry snow, and damp snow, and melted snow. Harusinec *et al.* [22] studied the design of equipment that simulates the environmental impact on the brake testing process. Henderson and Cebon [23] reviewed the emergency braking performance of a three-axle heavy truck semi-trailer on a wet basalt tile surface (similar to the ice surface), and used absolute error to measure the anti-skid ability of the brake system wheels. Pan *et al.* [24] studied the influence of driving habits on braking performance, and proposed a pressure control strategy for an integrated electro-hydraulic braking system. Zamzamzadeh [25] *et al.* studied the effect of brake pedal force on the braking distance of heavy vehicles under wet road conditions. Sharizli *et al.* [26] studied the impact of changes in vehicle dynamics (such as total vehicle weight, travel speed, and vehicle category) on the braking performance of heavy vehicles and their safe parking in emergencies. They studied a new method based on close tracking safety indicators.

From the research method of braking performance, Zamzamzadeh *et al.* [27] estimated the vehicle's slip distan-ce by performing a multi-body dynamics simulation on the vehicle. Suh *et al.* [28] showed a braking performance simulation on a semi-trailer tractor. Through the way of the power bonding graph in [29], J. Zhao *et al.* established a comprehensive nonlinear model of the braking system and evaluated the braking performance.

In summary, the researchers mainly think about the performance of the braking system from three aspects. Firstly, studying the structure, material, or static parameters of individual components in the braking system to find the optimal results, and improve the performance of the differe-nt parts to meet the braking requirements of the braking system. The individual components studied are mainly brakes, brake valves, charging valves, accumulators, etc. Secondly, through imaginative design or algorithm control, the key indicators that affect braking performance (such as: wheel-road adhesion coefficient, vehicle speed, braking force distribution, etc.) are studied. To achieve more accurate braking control, the researchers modified the system driving equation or transfer function. Thirdly, people considered the braking performance of the system under certain environmental operating conditions (such as vehicle load, slope, wind resistance, pedal displacement, driving habits, road conditions, etc.). From the existing research, the research generally adopts a single or a simple combination of the above three cases to study the braking performance of the braking system. It is challenging to concen-trate on the individual structural characteristics of the components, the matching of the braking system components, and the environmental working condition factors. Carrying out research and using a combination of the three to conduct systematic experimental research will make the work challenging to carry out and significantly increase the cost. Using system simulation to study the static and dynamic characteristics of braking performance in a comprehensive, time-saving, and economical manner, thus providing a reference to system design and experimen-tal prediction. Based on the extensive engineering applicati-on of Simcenter AMESim software in hydraulic system modeling and simulation, this article studies the braking performance of the conventional braking system of heavy vehicles.

The main contributions of this study are summarized as follows:

- We design a model of the closed-loop electro-hydraulic feedback charging valve, and consider the charging and discharging characteristics. This work provides a reference to the structural design and performance testing of a new charging valve.
- We establish a simulation model of wet multi-disc service brake. The influence of structural parameters of system components (brake valve) on brake perfor-mance is studied. We discuss the parameter matrix between the brake pedal and road adhesion coefficient, which can provide the prediction refers to the brake input in different subgrade environment.
- We explore the response of the vehicle load and slope to braking distance, deceleration, and brake temperature. The response of single axle braking and dual-axle braking is studied. It can provide references to vehicle braking response from a real environment.

The remainder of this article is organized as follows. Section II briefly analyzes the service brake of heavy vehicles (wheel loader), and designs a new type of charging valve. Section III theoretically discusses the force balance and moment balance under general working conditions. The major part of this work focuses on the modeling and simulation of the brake system of the loader, and gives the simulation results (Section IV). Finally, conclusions are drawn in section V.

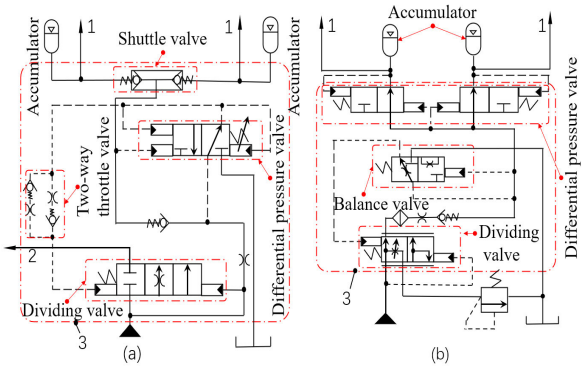

FIGURE 1. Two typical double-circuit charging circuit.

II. ANALYSIS OF SERVICE BRAKE

We consider the wheel loader as an example. It's service brake mainly includes a charging circuit and a brake circuit.

A. CHARGING CIRCUIT

The charging circuit is mainly composed of a hydraulic source, a charging valve, an accumulator, and its piping accessories. The typical brake valves currently on the market are Rexroth brake valves and MICO brake valves, as shown in Fig. 1. In Fig.1 (a), the charging valve includes a dividing valve, a differential pressure valve, a shuttle valve, and a two-way throttle valve. The dividing valve mainly realizes the switching of the spool in three stations through the pressure feedback from the left and right ends. The pressure on the dexter end of the dividing valve is the pressure on the outlet of the constant flow source. The difference, which is between the set pressure on the right end of the differential pressure valve and the feedback pressure of the primary oil circuit on the left end, determines the stress on the left end of the dividing valve. During the charging phase of the accumulator, the pressure on the left end of the differential pressure valve is less than the dexter end Pressure. The left position of the differential pressure valve works, and the spool of the dividing valve is in the left position cut-off state. Consequently, the main oil path is turned on. Along with the pressure of the accumulator increases, the pressure on the left end of the differential pressure valve is higher than the right-hand end Pressure. The dexter position of the differential pressure valve works, the high-pressure oil signal of the leading oil circuit is fed back to the left end of the dividing valve through the feedback circuit of the differential pressure valve. The spool of the dividing valve moves to the center or right station so that the primary channel stops filling. And then, the flow of the constant current source flows to other circuits. In the discharge phase, as the high-pressure oil of the accumulator is released to the brake circuit several times, the feedback pressure on the left end of the differential pressure valve will continue to decrease. When the pressure is lower than the set pressure on the right-hand end of the differential pressure valve, the spool of the differential pressure valve will move to the left. And then, the primary oil circuit is reconnected to the charging stage.

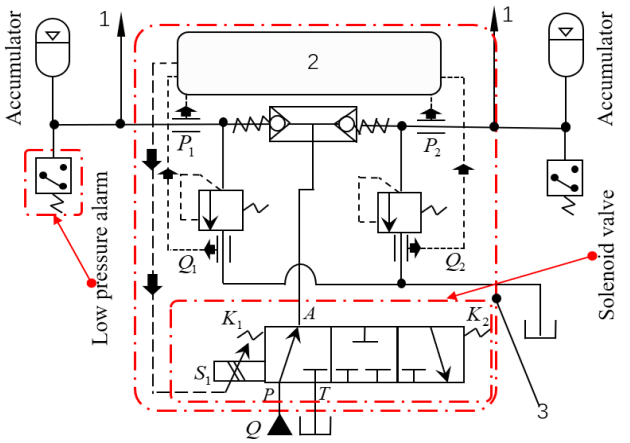

FIGURE 2. A new type of charging valve dual- circuit charging.

The basic working principle of Fig. 1 (b) is similar to that of Fig. 1 (a). When the accumulator is in the charging stage, the right station of the balance valve works, and the left station of the shunt valve works as the leading oil circuit continues to supply oil, the accumulator charging pressure and the main oil circuit pressure increase. When the pressure in the primary oil circuit rises to make the spool of the differential pressure valve switch, the accumulator will be filled with oil. The closed state of the differential pressure valve instantly increases the pressure in the primary oil circuit, causing the balance valve to switch to the left position. Then, the stress in the central oil circuit is fed back to the left end of the dividing valve. The spool of the dividing valve moves to the right-hand to achieve the main oil circuit diversion. When the accumulator is discharged enough to make it communicate with the primary oil circuit, the spool of the balance valve will return to the right-hand position. At the same time, the dividing valve will also respond to the left-hand station and return to the accumulator charged state.

Therefore, the charging valve is essentially a full-hydraulic closed-loop feedback check valve with the characteristics of hydraulic feedback and check valve. Compared with the full hydraulic control, a wire-controlled electro-hydraulic transmission has the advantages of quick response, excellent real-time performance, and easy integration [14]. In terms of structure, the structure is more straightforward and more comfortable to manufacture. In terms of control performance, hydraulic control feedback has pressure loss along the pipeline, and the response hysteresis is not easy to adjust, while electro-hydraulic feedback can achieve pressure compensation or correction through algorithms. On the whole, the electro-hydraulic transmission is more suitable for the intelligent and integrated development of today's construction machinery. Consequently, we design a new charging valve based on electro-hydraulic closed-loop feedback, as shown in Fig. 2. The basic working principle is that when the pressure sensor in the double circuit collects either accumulator pressure lower than the lower-pressure limit set by the pressure comparator, the spool of the three-position

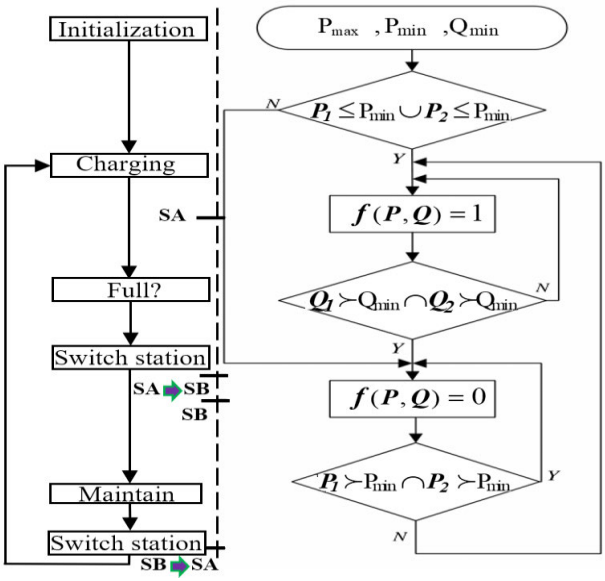

FIGURE 3. Control signal of the three-position three-way valve.

three-way solenoid valve is switched to the left station. The charging valve will automatically charge the accumulator with oil and replenish energy. When the charging pressure of either circuit reaches the upper-pressure limit set by the pressure comparator, the spool of the three-position three-way solenoid valve is switched to the neutral or right position, and the charging valve stops charging.

In Fig. 2, whether the accumulator is filled depends on the pressure difference between the working pressure and the set lower pressure limit. Firstly, assuming that the working pressure is within the set pressure range, the accumulator will not be charged with oil. However, along with the pressure energy is supplied to the brake circuit, the accumulator press-ure will continue to decrease. Secondly, when it drops to the lower-pressure limit set by the pressure comparator, the charging circuit will start to work. The charging valve will keep charging until the pressure of both accumulators reaches the upper-pressure limit set by the pressure comparator.

Fig. 3 presents the control flow block diagram. SA represents the left station of the three-position three-way solenoid valve in Fig. 2, and SB represents the middle or dexter station. Adopting medium flow (50 L/min) fast liquid supply and ignoring the process factors of spool opening and closing, and the essential expression of the control signal is as follows:

$$f(P,Q) = \begin{cases} 1 & (P_1 \le \mathrm{P_{min}} \cup P_2 \le \mathrm{P_{min}}) \text{ to } (Q_1 \succ \mathrm{Q_{min}} \cap Q_2 \succ \mathrm{Q_{min}}) \\ 0 & \text{the other} \end{cases} \tag{1}$$

Among them, $f(P, Q)$ is the opening degree of the three-position three-way valve port, P_1, P_2, and $\mathrm{P_{min}}$ respectively, are the collected values of the two-way pressure sensors and the minimum amount of the set pressure. Q_1, Q_2, and $\mathrm{Q_{min}}$ respectively, are the obtained value of the two-loop flow sensors and the set minimum value of overflow.

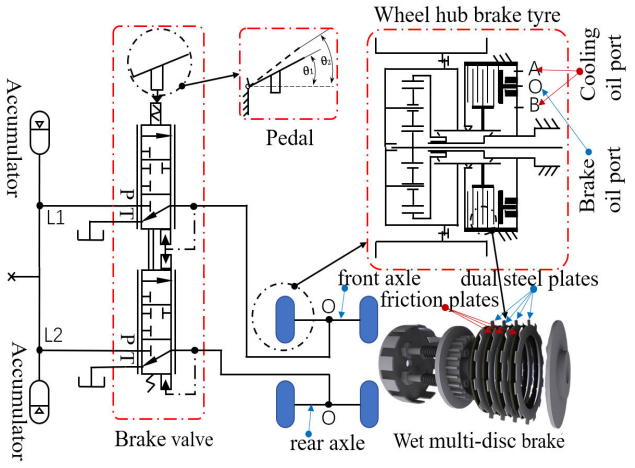

FIGURE 4. Brake circuit.

B. BRAKE CIRCUIT

As shown in Fig. 4, the brake circuit is mainly composed of two accumulators, a brake valve, four wet multi-disc brakes, and its pipeline accessories. Among them, the wet multi-disc brake plays an essential role in the braking process, which has several steel plates and friction plates interleaved. The friction plates are connected with the rotating axle shaft or hub by spline, while the steel plates are fixed in the groove of the axle housing along the half axis direction. When braking is required, the operator steps on the brake valve pedal, and the high-pressure oil in the two accumulators flows into the brakes of the front and rear axles, respectively. The high-pressure oil in the brake pushes the piston ring to press the dual steel discs and friction discs against each other to generate a braking torque.

During the i-th release of the accumulator, assuming that the volume flow of the oil released is ΔQ_i, the accumulator outlet pressure changes from P_{1i} to P_{2i}, and the pressure behind the brake valve is P_{3i}. Then the average flow rate of every brake obtained from the pressure-flow equation is:

$$q_i = \frac{1}{2}\Delta Q_i = \frac{1}{2} c_q x w \sqrt{\frac{2}{\rho}\Delta P_i} \tag{2}$$

Among them, c_q is the flow coefficient, x is the opening degree of the brake valve port, w is the area gradient of the brake valve port, ρ is the oil density, $\Delta P_i = P_{3i} - P_{2i}$, $i \in (0, n]$, and n is the maximum number of braking times that the accumulator can provide in a braking cycle.

In the tandem brake valve structure shown in Fig. 4, L1 and L2 represent the front and rear axles, respectively. The hydraulic feedback of the front axle plays a role in banlanc-ing the spool and transmitting power. The rear axle hydrau-lic feedback mainly plays a role in brake awareness. The brake valve balance equation is:

$$\ddot{y} = \frac{1}{\mathrm{m}}(F - \mathrm{B}\dot{y} - \mathrm{k}(\mathrm{y_0} + y) - \frac{\pi d^2}{4} P_{3i}) \tag{3}$$

where y is the spool displacement, m is the spool mass, F is the sufficient external force of the pedal on the spool, B is the

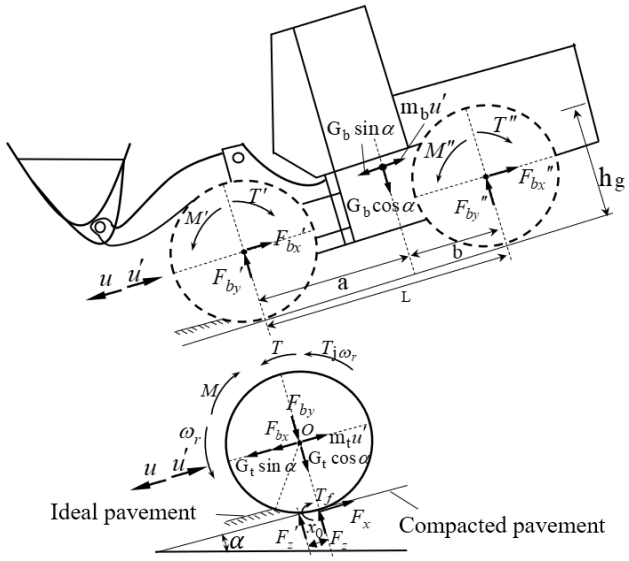

FIGURE 5. Wheel force braking model.

spool damping coefficient, k is the return spring stiffness, y_0 is the pre-compression of the spring, d is the spool diameter at the feedback end of the rear axle.

The wet multi-disc brake belongs to disc friction, and the friction braking torque of the brake-based on the principle of constant wear is as follows:

$$M_{\mathrm{b}} = \frac{1}{2}\mu_{\mathrm{disc}} z F_N (r_1 + r_2) \tag{4}$$

In the formula, M_{b} is the friction torque received by a single brake, μ_{disc} is the dynamic friction factor of the friction disc, z is the number of friction surfaces, F_N is the vertical pressure on the friction surface, r_1 is the inner radius of the friction disc, and r_2 is the outer radius of the friction disc.

III. MECHANICAL ANALYSIS

A. DRIVING FORCE ANALYSIS

As shown in Fig. 5, it shows the stress state of the whole vehicle and single wheel during the braking process of the dual-axle wheel loader, ignoring the wind resistance. Among them, u, u', and ω_r are the speed, deceleration and angular velocity of the vehicle or wheel respectively, M, M', M'', T, T', and T'' are respectively the braking torque and driving torque of the single tire, the front axle of the vehicle, and the rear axle of the vehicle, $T_{\mathrm{j}\omega_r}$ and T_f, respectively, are the moments of inertia and rolling resistance, $F_{b_x}, F'_{b_x}, F''_{b_x}, F_{b_y}, F'_{b_y}$, and F''_{b_y} are the forces that the body exerts on the wheels and the wheels react to the body along the slope and perpendicular to the hill. α is an incline angle. a is the distance from the center of gravity of the vehicle to the front axle, b is the distance from the center of gravity of the whole vehicle to the rear axle, L is the distance between the front axle and the rear axle, r is tire radius, $\mathrm{G_b}$ is the weight of the entire vehicle, $\mathrm{G_t}$ is the weight of individual wheels, $\mathrm{m_t}$ is the mass of a single wheel, $\mathrm{m_b}$ is the mass of the whole vehicle, $\mathrm{h_g}$ is the height from the center of gravity of the vehicle to the compacted road surface, x_0 is the distance between the actual tire fulcrum and the ideal rigid contact point. F_x, F_z and F'_z are respectively the rolling friction force, the force at the ideal position, and the force at the actual position. μ_{road} is the rolling friction coefficient between the wheel and the road surface.

Along the inclined direction, the balanced equation of the transverse force at the wheel center is:

$$F_x - \mathrm{G_t}\sin\alpha - F_{b_x} - \mathrm{m_t}u' = 0 \tag{5}$$

In the above formula, F_{x} is the sliding friction force. However, $F_{\mathrm{x}} = \mu_{\mathrm{road}}(\mathrm{G_t}\cos\alpha + F_{b_y})$, so the equation above can also be written as

$$\mu_{\mathrm{road}}(\mathrm{G_t}\cos\alpha + F_{b_y}) - \mathrm{G_t}\sin\alpha - F_{b_x} - \mathrm{m_t}u' = 0 \tag{6}$$

Perpendicular to the direction of the inclined plane, the longitudinal force balance equation of the wheel center is:

$$F_z - \mathrm{G_t}\cos\alpha - F_{b_y} = 0 \tag{7}$$

The balanced equation of the wheel center torque is:

$$T_f + M - T - T_{\mathrm{j}\omega_r} - F_x \cdot \mathrm{r} = 0 \tag{8}$$

The rolling resistance torque of the wheel is:

$$T_f = (\mathrm{G_t}\cos\alpha + F_{by}) \cdot x_0 \tag{9}$$

For the whole loader:

Along the slope direction, the vehicle transverse force balance equation is:

$$F'_{b_x} + F''_{b_x} - \mathrm{G_b}\sin\alpha = \mathrm{m_b}u' \tag{10}$$

The equation of the vehicle torque balance at the center of the front wheel is:

$$F''_{b_y}\cdot\mathrm{L} + M' + M'' - T' - T'' - \mathrm{G_b}\cos\alpha\cdot\mathrm{a} - \mathrm{m_b}u'\cdot(\mathrm{h_g} - \mathrm{r}) = 0 \tag{11}$$

The moment balance equation of the whole vehicle in the center of the rear wheel is as follows:

$$F'_{b_y}\cdot\mathrm{L} - M' - M'' + T' + T'' - \mathrm{G_b}\cos\alpha\cdot\mathrm{b} + \mathrm{m_b}u'\cdot(\mathrm{h_g} - \mathrm{r}) = 0 \tag{12}$$

B. THERMAL ANALYSIS

When cutting off the power system, the leading residual energy of the system comes from the mechanical power of the system (including the translational kinetic energy of the vehicle, the rotational kinetic energy of four wheels, and the potential energy of the vehicle). Compared with the inclined reference system (inertial reference system), the residual mechanical power of the system converts into the mechanical energy dissipation, and the potential energy of the vehicle. The dissolution of mechanical energy occurs in the place where the relative displacement changes during braking, such as the relative sliding between the friction plate and the dual steel plate in the brake, and the wheel relative to the ground, etc. Studies have shown that [6], friction braking and gear engagement in the brake consume almost all mechanical energy dissipation, while the friction produced by the friction plate and the dual steel plate in the brake absorbs about 90%

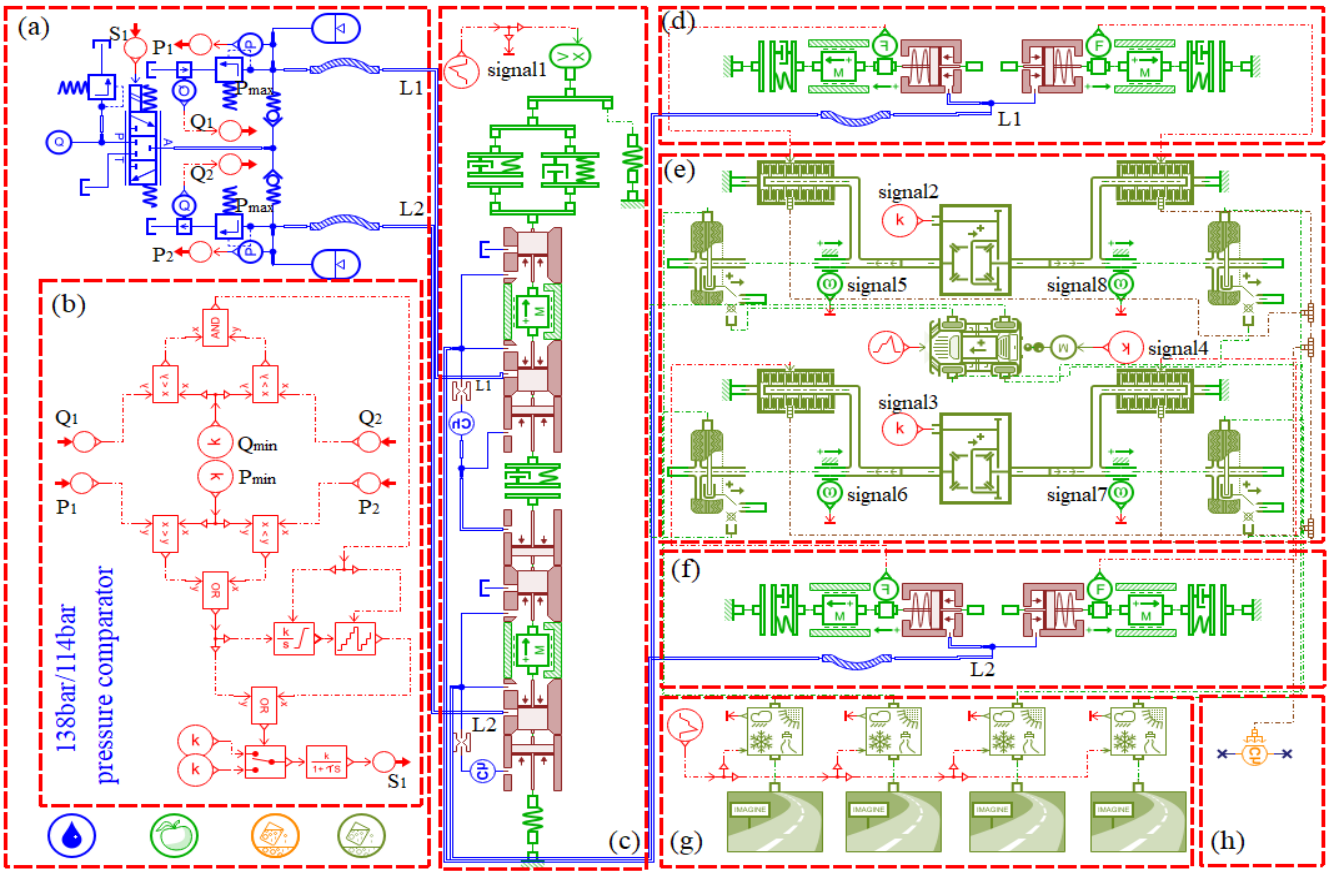

FIGURE 6. Wet multi-disc service brake.

of the mechanical energy dissipation and converts it into thermal energy. Therefore, the heat of formation is:

$$Q_{\text{brake}} = \mathrm{C}\left(\frac{1}{2}\left(\mathrm{m_b}+\Delta m\right)u(t_1)^2+2\mathrm{J}\omega_r(t_1)^2-\left(\mathrm{m_b}+\Delta m\right)\mathrm{g}\Delta h\right) \tag{13}$$

where Q_{brake} is the braking heat generated, C is the heat generation ratio, Δm is the loading mass of the vehicle, and $u(t_1)$ as described above is the vehicle driving speed at the moment t_1 in the direction of motion, and J is the rotational inertia of a single wheel, $\omega_r(t_1)$ is the average speed of the wheel at the moment t_1, g is the local gravity acceleration, and Δh is the relative height difference of the vehicle.

IV. MODEL AND SIMULATION ANALYSIS

In Fig.6, we establish a simulation model of the wet multi-disc brake system with a new charging valve structure in the simcenter AMESim 16.0 environment. (a) is the accumulat-or charging circuit, (b) is the pressure comparator, (c) is the tandem brake valve, (d) is the brake wheel cylinder of the front axle, (e) is the four-wheel-drive whole vehicle (including front axle, rear axle, body), (f) is the brake wheel cylinder of the rear axle, (g) is the ground, and (h) is a self-cooling hot liquid chamber. L1 and L2 respectively represent the front axle and the rear axle. A hose connection is used between (a) and (c), and also between (c) and (d).

TABLE 1. Key parameters of charging circuit.

Parameter	Value	Reference
Hydraulic source (L/min)	50	ref[10]
Overflow $Q_{\min}$ (L/min)	10^{-5}	--
Maximum pressure $P_{\max}$ (bar)	138	MICO06-463-200
Minimum pressure $P_{\min}$ (bar)	114	MICO06-463-200
Accumulator ×2 (L)	4	NXQAB-4/20-L-A
Gas pre-charge pressure (bar)	100	ref[10]
System overflow pressure (bar)	210	–
First-order inertial gain	40	--

A. CHARGING AND DISCHARGING CHARACTERISTICS

The charging circuit is composed of (a) the accumulator charging circuit and (b) the pressure comparator in Fig.6, and the pressure comparator transmits the charging signal to the three-position three-way solenoid valve, to implement the charging of the two-way accumulator. Based on the engineering practice and references of the ZL50 loader, the critical parameter settings of the charging circuit are shown in TABLE 1.

The response curve of the dual-channel accumulator at different initial pressures is shown in Fig. 7 (a). The response time of the accumulator is about 2.3s for the first time from one atmosphere to the upper limit of the pressure setting 138bar. After the accumulator usually works, the response

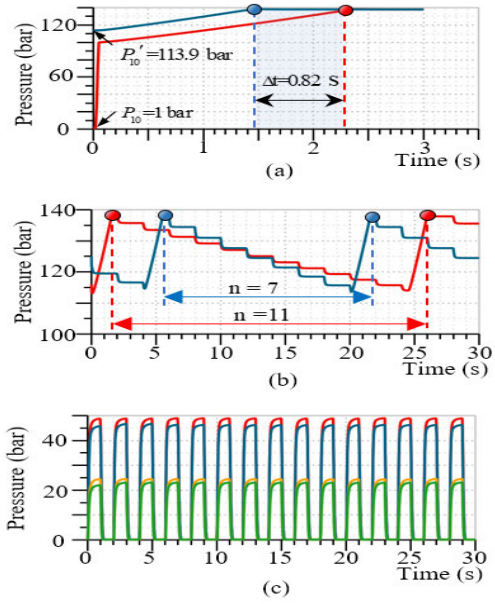

FIGURE 7. Response curve of accumulator.

time from oil replenishment to the upper-pressure limit is about 1.5s, and the response time difference between the two is about 0.8s; Fig. 7 (b) and (c) show that the discharge process of the accumulator with an output pressure of about 24bar and 48bar, respectively. When the output pressure is 24bar, the accumulator can discharge oil for a maximum of 11 times in a charging-discharging cycle, and when the output pressure is 48bar, the accumulator can release the liquid for a maximum of 7 times in a charging-discharging period.

In Fig.8, the rising edge of the a1 signal represents the transition of the accumulator pressure($P_1 \leq P_{min} \cup P_2 \leq P_{min}$) from logical truth to logical false, so that the charging value is within the upper and lower limits of the accumul-ator pressure without stopping the charging signal, only when b1 sends out the message, a1 stops working. A2 represents the status signal of the whole charging phase. When the two accumulators are full of oil, b1 immediately sends a signal to reset a1 and a2 to prepare for the next charging. C1 is a signal of a three-position three-way solenoid valve. The rising and horizontal phases of the curve indicate that the accumulator is charging. The descending phase of the curve indicates that the accumula-tor has completed filling. Signal value = 0 indicates that the accumulator is not charged. C2 and c3 represent accumulator pressure and charging valve inlet pressure, respectively. The accumulator is filled quickly, and its discharge can last several times. When the pressure of the accumulator is lower than a particular value, the charging valve can recharge the accumulator again.

B. THE CHARACTERISTICS OF BRAKE VALVE

As shown in Fig. 6, the brake valve is the structure of upper and lower valve cores in series. The initial simu-lation parameters in TABLE 2. The basic settings of the brake valve directly affect the pressure output characteristics.

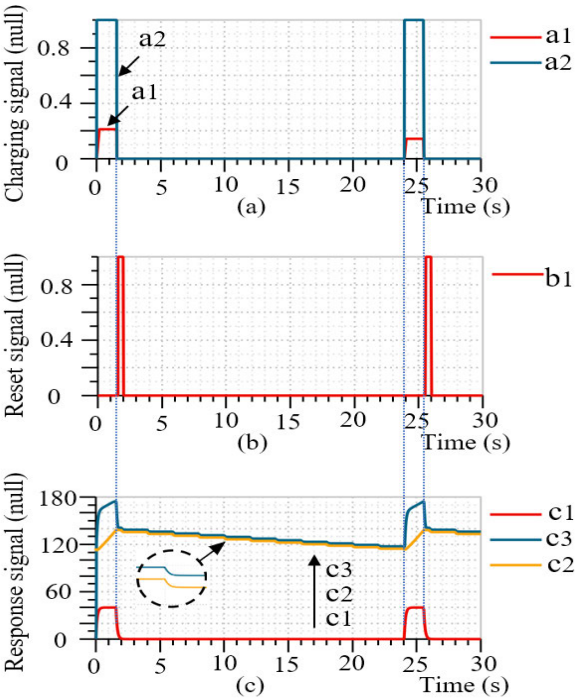

FIGURE 8. Signal response of pressure comparator.

TABLE 2. Parameters of brake BAVLE.

Legend	Parameter	Value
	Pedal step signal (null)	3.5e-2
	$\mathcal{A}$: Spring rate(N/m)	6e+4
	$\mathcal{B}$: Contact stiffness(N/m)	4e+4
	$\mathcal{C}$: Spool/ Rod diameter(mm)	20/5
	$\mathcal{D}$: Lower displacement limit(m)	-1.5e-2
	$\mathcal{D}$: Higher displacement limit(m)	1e-3
	$\mathcal{E}$: Spool diameter(mm)	20
	$\mathcal{E}$: Underlap (mm)	-8
	$\mathcal{F}$: Orifice geometry diameter(mm)	0.8
	$\mathcal{G}$: Spool/ Rod diameter(mm)	10/5
	$\mathcal{H}$: Spring rate(N/m)	1e+5
	$\mathcal{H}$: Return spring initial pressure(N)	200

Fig. 9 and Fig. 10 show the effect of different parameter gradie-nts of the brake valve to the output pressure characteristics.

In Fig.9, (a)-(d) are the response curves of wheel cylinder pressure with a pedal signal. The pedal signal values set are 0.02, 0.035, 0.05, and 0.06, respectively. In Fig. (b), the greater the pedal signal value, the faster the response of the spool and the longer the valve opening time. In Fig. (c), the second quadrant is the point brake zone, the size of the area reflects the maximum stroke of the pedal and the speed response of the valve core. The greater the pedal travel, the larger the point braking area and the more braking points. In Fig. (d) as the pedal signal values increases, the output pressure of the wheel cylinder increases, and the response time becomes longer, and it will remain unchanged after reaching a certain pressure value. Figs. (e)-(h) show the

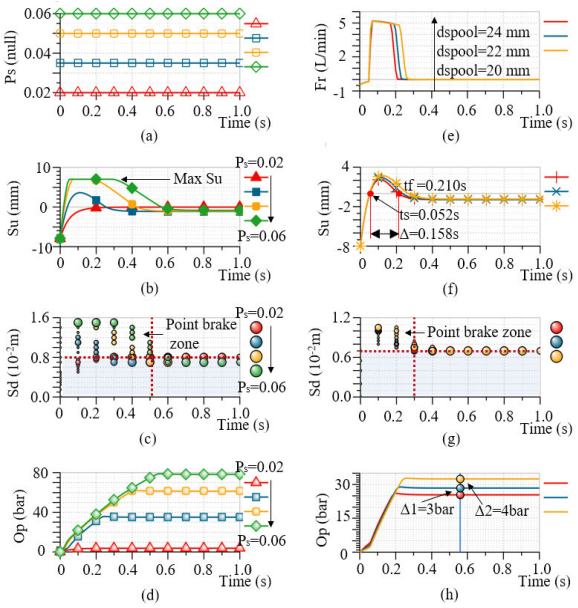

FIGURE 9. Response caused by pedal signal and spool diameter.

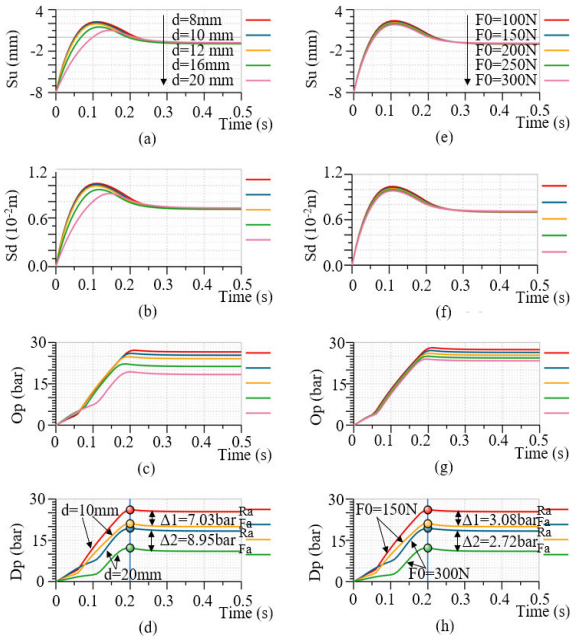

FIGURE 10. Output response curve.

response curves of the wheel cylinder pressure. Assuming the pedal signal is 0.03, and the large diameter of the valve spool is 20mm, 22mm, and 24mm, respectively. In Fig. (e), the flow rate increases with the value of the spool diameter, and there is almost no time difference during the opening of the spool. During the rebound of the spool, the larger the diameter of the spool, there is a short spool closing lag. In Fig. (f), the spool flow opening time is about 0.052s, and the spool opening to closing response time is about 0.158s. In Fig. (g), the density area of the point brake zone reduced compared with Fig. (c). This area reflects that an ability to adjust the brake range by changing the brake valve core is weakened.

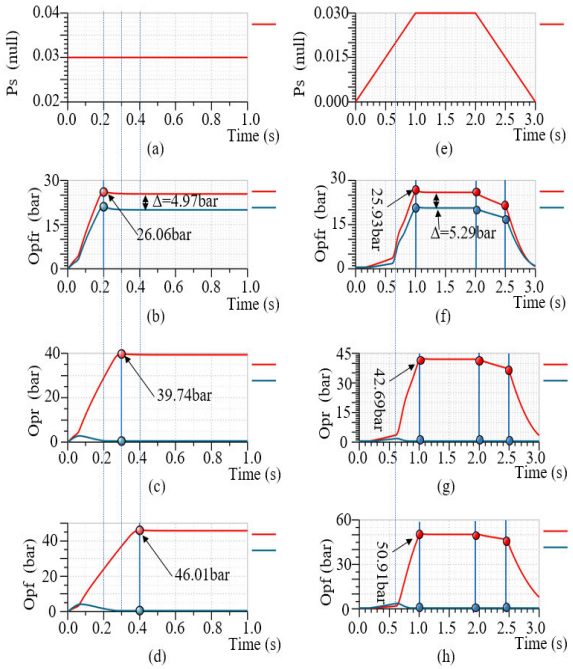

FIGURE 11. Single axle braking and dual-axle braking.

In Fig. (h), the slope of the pressure response is almost unchanged. After reaching equilibrium, the pressure value is stable and unchanged. When the base spool diamet-er value is 20mm, the output pressure increases by approxi-mately 3 to 4bar for every 2mm increase in spool diameter.

In Fig.10, (a)-(d) are the output response caused by the change in the cross-sectional diameter of the rear axle spool. The gradient of the change is from 8 mm to 20 mm. In Figs. (a)-(c), as the spool cross-sectional diam-eter increases, the spool opening displacement reduces, the response lags, the brake wheel cylinder pressure changes significantly. When the time above about 0.2s, the output pressure is stable after the spool is closed, and there is no noticeable spool closing lag. Fig. (d) shows the pressure difference between the front and rear drive axles when the diameter of the spool section is 10mm and 20mm, respec-tively. When the cross-sectional diameter of the rear axle spool redoubles, the pressure difference increases by 2bar. Figs (e)-(h) show the output response caused by the change of the preload force gradient of the return spring. The gradient is from 100N to 300N. From Fig. (e) to Fig. (g), we can see that the change in the preload gradient has a small change in the amount of underlap, displacement, and wheel cylinder pressure output of the brake valve spool, with no discernible effect. When the return spring preload is 150N or 300N in Fig. (h), there is no visible change in the pressure difference. Whether it's front or rear, the pressure difference of the brake wheel cylinder is about 3bar, and the pressure difference is small-er than that in Fig. (d).

In Fig.11(a)-(d), under the step signal, the dual-axle pressure difference is about 5bar, the highest stable output of the rear axle pressure is 26.06bar, and the permanent response

TABLE 3. Basic parameters of vehicle.

Parameter	value
The vehicle Mass (empty/full load) (kg)	16800/21800
Road slope (%)	-58-58
The range of surface adhesion coefficients (null)	0.1-0.8
Initial ambient temperature (°C)	20
The wheel radius(m)	0.75
Wheel inertia(kg*m^2)	133.3
Initialising speed (km/h)	32

TABLE 4. Brake parameters.

Parameter	value
The number of spring(null)	8
Preload of a single spring(N)	75
Piston movement distance(mm)	3.75
Return spring of brake coefficients K(N/mm)	21

time is 0.2s. When only the rear-drive axle brakes, the stable pressure output of the rear axle is 39.74bar, and the response time is 0.3s. When only the front drive axle brakes, the firm output pressure is 46.01bar, and the response time is 0.4s. In Fig.11(e)-(h), under the step signal input, within 0-1s, there is a slow zone in the output pressure response. When the dual-axle brake responds, the pressure difference between the front and rear drive axles is about 5bar, and the highest stable output of the rear axle pressure is 25.93bar, which is equivalent to Fig. (b). When only the rear axle is working, the output pressure is 42.69 bar, and when only the front axle is working, the output pressure is 50.91bar. Therefore, under the step signal, the brake pressure output response is the fastest, and the requir-ed pressure is small, followed by the rear axle response, and finally, the front axle response. Under the step signal, there is no response lag in the three cases, only the difference in output pressure.

C. BRAKING ANALYSIS OF THE WHOLE VEHICLE

For the whole vehicle braking, the fundamental parameters set are shown in TABLE 3 and TABLE 4.

In Fig.12, under the conditions of full load, flat road, and initial vehicle speed $v_0 = 32$km/h, the effect of the 8 * 8 matrix parameter composed of the brake valve pedal signal and road adhesion coefficient on the braking distance is studied. The range of the pedal signal is [0.01, 0.08], and The scope of the road adhesion coefficient is [0.1, 0.8]. In Fig. (a), the maximum braking distance is determined according to the ISO3450-85 standard, and the red area of the parameter matrix is determined as the brake safety area according to the simulation, that is, when $Ps \in [0.03, 0.08]$ and $K \in [0.3, 0.8]$, the braking distance is less than the standard displacement. The black frame is the braking safety comfort zone, that is, when $Ps = 0.03$ and $K \in (0.5, 0.8]$ or $Ps \in [0.03, 0.08]$ and $K \in [0.3, 0.5]$, the deceleration is less than or equal to 4m/s^2, and it belongs to the braking safety zone. In Fig. (a), the shortest braking distance is about 8.3m, the shortest braking time is 1.34s, and the braking interval threshold is 15.24m.

Fig. (b), (c), and (d) reflect the change in coefficient with the braking distance when the pedal signal is 0.05.

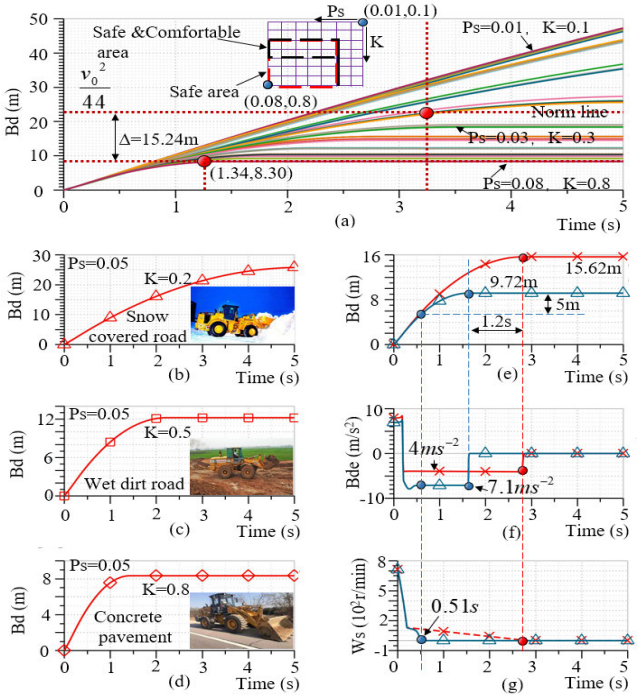

FIGURE 12. Braking distance response caused by Ps and K.

On snowy roads, the wheel loader can't brake within 5 seconds, and (c), (d) represent wet earth roads and concrete roads, and the horizontal line represents that the vehicle has achieved braking at a particular time. In Figs (e)-(g), the braking comfort is discussed. When the deceleration is greater than or equal to 7m/s^2, it represents emergency braking. When the deceleration is about 4m/s^2, it represents standard braking. When it's about at 0.51s, the wheel speed is 0, and the vehicle stops at about 1.61s. At this stage, the vehicle has sliding friction, the friction sliding distance is 5m, and the final total braking distance is 9.72m. With 4m/s^2 braking, we can see from the Fig (g) that there is no relative slip during the entire braking process, and it is relatively stable. The final braking distance is about 15.62m, which meets the braking requirements.

Fig. 13 studies the effects of load, road adhesion coneffici-ent, and slope on vehicle braking kinematics. Suppose $Ps = 0.04$, the initial speed is $v_0 = 32$km/h, the slope range is $[-30°, 30°]$, and the variation range of road adhesion coefficient is [0.1,0.8]. Figs. (a)-(c) respectively represent the instantaneous braking displacement, speed, and deceleration of the wheel loader under different working conditions at 5s. The figure of full vehicle load (indicated by the red map in Fig.13) almost coincides with the character of no-load vehicle. In (a) - (c), the local red area on the upper surface represents that the output response at full load is slightly higher than that at no-load under the same conditions.

When the adhesion coefficient and slope value are in the lower triangle area (uphill section), that is, the adhesion coefficient $K \in [0.1, 0.5]$ and slope range is $[0, 30°]$. At this time,

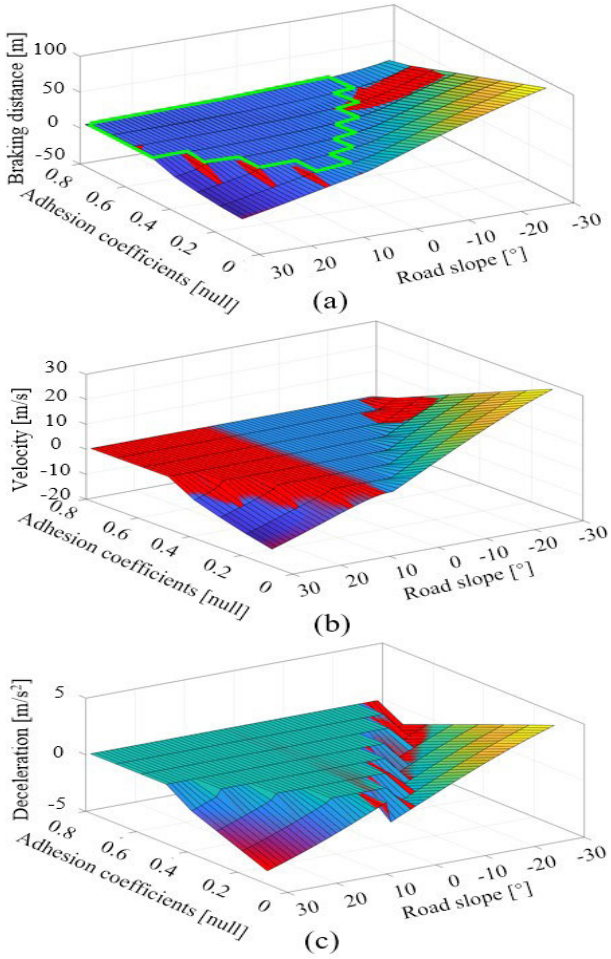

FIGURE 13. Kinematics map of vehicle braking.

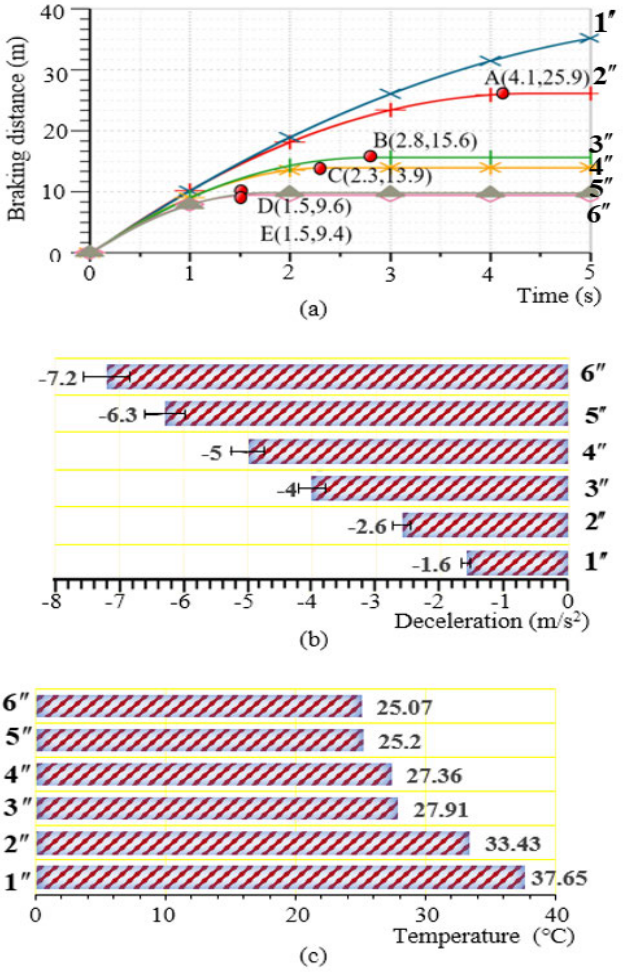

FIGURE 14. The effect of load and slope on braking distance, deceleration, and temperature rise.

the vehicle will slip and reverse after braking. When the adhesion coefficient and slope range are in the upper triangle region (downhill section), that is, the adhesion coefficient $K \in [0.1, 0.8]$. The slope range is $[-30°, 0]$. At this time, the vehicle cannot be braked with the increase of slope, the adhesion coefficient decreases, and the displacement, velocity, and acceleration of the vehicle increase. Other areas (such as inside the green wireframe in Fig. 13 (a)) can realize braking smoothly.

Assuming that the loader works in a dry native soil environment, K = 0.65, Ps = 0.03, and the initial temperature is set to 20 °. Fig. 14 shows the braking distance, deceleration, and the brake self-cooling temperature of the loader under normal conditions. In (a)-(c), We can speculate that the higher the load and the smaller the slope value, the higher the moving distance of the loader, the smaller the deceleration, and the higher the temperature. With the increase of slope value, the influence of load on the moving distance will be smaller, the deceleration will increase, and the temperature will decrease.

As shown in Fig. 15, the self-cooling cavity in Fig. 6 is replaced by the one with forced cooling. Fig.16 lists the comparison of the temperature when the brake is balanced

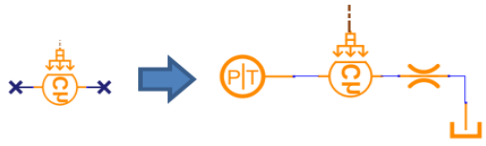

FIGURE 15. Self-cooling and forced cooling.

in the two cooling methods. It can be found that under the same slope and the same load, the equilibrium temperature of the brake with forced cooling is lower than that of the self-cooled brake. Overall, the temperature is the highest when braking downhill at full load. The temperature rise is the lowest when braking uphill with a full load.

D. CYCLE CONDITION ANALYSIS

The working methods of the loader are mainly "V", "L", "I" and "T". No matter which working method, the loader brakes twice at full load and twice at no load in one working cycle. The braking signal of (c) and the speed signal of (e) in Fig. 6 are connected to the input/output module of the cycle condition in Fig. 17, namely, sign1, sign5, sign6, sign7, and sign8 are input signals, and sign4 is the full load

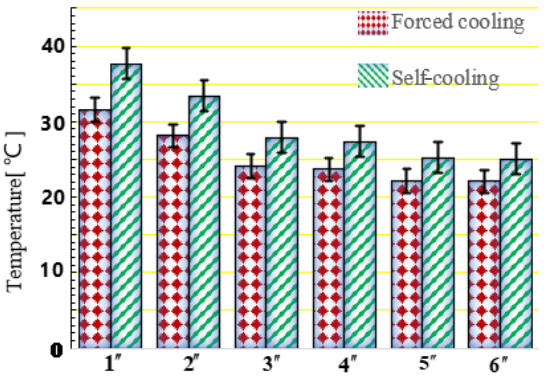

1″ : Load = 5000 kg, slope = -14°, 2″ : Load = 0 kg, slope = -14°, 3″ : Load = 5000 kg, slope = 0°, 4″ : Load = 0 kg, slope = 0°, 5″ : Load = 0 kg, slope = 14°, 6″ : Load = 5000 kg, slope = 14°

FIGURE 16. Comparison of brake temperature.

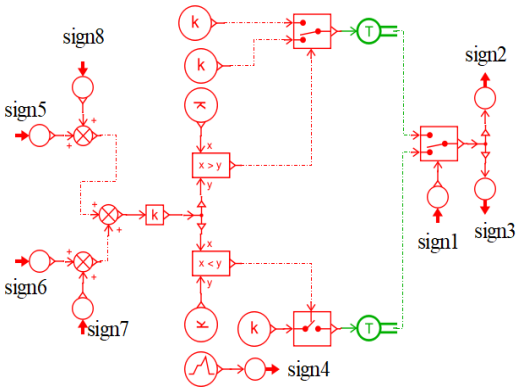

FIGURE 17. Cycling mode input and output module.

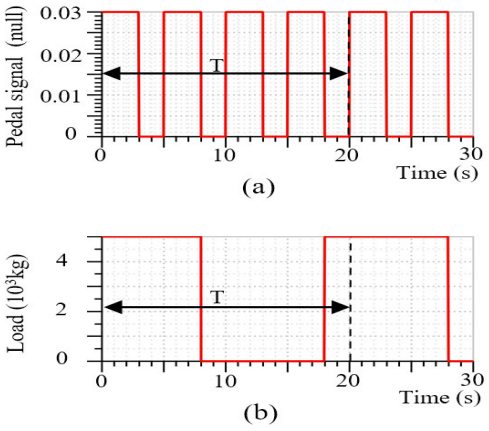

FIGURE 18. Brake signal and load signal.

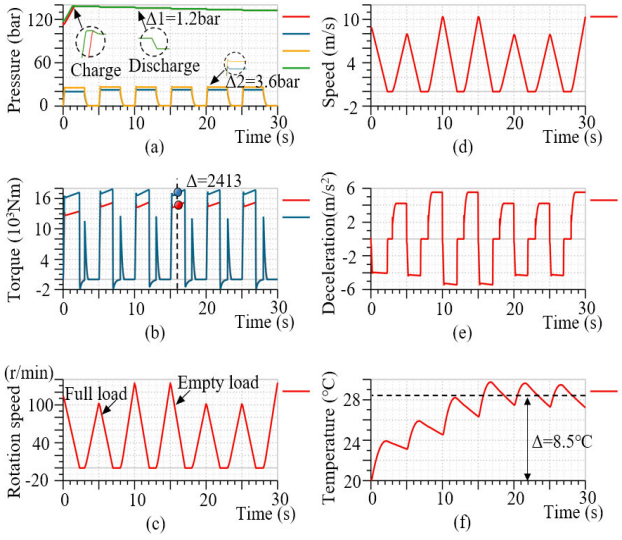

FIGURE 19. Response curve within 1.5 cycles.

or no-load of the loader in the cycle Carrying message, sign2, and sign3 are the input driving torque of front axle and rear axle of (e) in Fig. 6.

According to the study of the loader without sliding brake in the native soil working environment, that is, the road adhesion coefficient K = 0.65 and the point brake signal Ps = 0.03, and the loader full load and no-load signal as shown in Fig. 18. The cooling system uses forced cooling to exchange heat.

Fig.19 shows the output response curve in 1.5 cycles. In Fig. (a) the front and rear drive axle accumulators are filled at the beginning, and then the accumulator is discharged. The working pressure of the rear axle is 3.6 bar higher than the working pressure of the front axle. Fig. (b) shows dual-axle braking torque, the torque difference is about 2413 Nm. Fig. (c) shows the speed response of the wheel under no-load and full load. The wheel speed decreases with time to indicate the braking process, and the wheel speed increases with time to mention the starting process. The maximum speed of the wheel when the load is running is about 40r / min lower. Fig. (d) and Fig. (e) show the speed curve and acceleration curve of the loader. The maximum speed at no load is about 36 km/h. The braking deceleration is about 5m/s^2, and the maximum speed at full capacity is about 29 km/h, the braking deceleration is about 4m/s^2. Fig. (f) shows that the brake temperature rises about 8.5 °C in 1.5 cycles, and the brake temperature tends to stabilize after one brake cycle.

V. CONCLUSION

(1) This article creates a new charging valve based on electro-hydraulic closed-loop feedback, and establish a feedback signal circuit of the pressure comparator. The charging characteristics of the dual-circuit composed of a new filling valve were studied. The first charge of a 4L accumulator requires 2.3s. After the accumulator usually works, the response time from the lower pressure limit to the upper-pressure limit is about 1.5s. The response time difference between the two is about 0.8s.

(2) The simulation model of the wet multi-disc service brake is established, and the output response of the static structure parameters of the tandem brake valve to the brake pressure is studied. There are four conclusions. First, in the response of the pedal signal, spool diameter, rear axle spool section diameter, and return spring preload to

the output pressure, the pedal signal has the most apparent change in the brake output pressure; the second quadrant represents the braking area. The higher the density of the braking zone, the more braking points, the higher the pedal travel, and the more influential the braking capacity. Second, the spool diameter does not affect the spool flow opening time, and there is no output hysteresis response, but during the spool rebound process, the larger the spool diameter, the spool flow closure will lag. Third, the cross-sectional diameter of the rear axle spool affects the output response time. There is a response lag, but there is no noticeable spool closing lag during the spool rebound. Finally, the adjustment capacity of the return spring preload is weak, and there is no noticeable change in the output pressure.

(3) Among the dual-axle and single-axle brakes, the dual-axle brake has the fastest response, followed by the rear axle, and finally the front axle. The dual-axle brake has the lowest base pressure, followed by the single-axle rear axle, and finally, the single-axle front axle.

(4) The effect of the 8 * 8 matrix parameter composed of the brake valve pedal signal and road adhesion coefficient on the braking distance is studied. And the parameter ranges of the braking safety zone and braking safety comfo-rt zone are obtained. The braking conditions of snowy roads, wet earth roads, and concrete roads were studied.

(5) The effects of slope, road adhesion coefficient, and load on the braking distance, braking speed, deceleration, and brake temperature are studied. Research shows that when the loader is downhill and full capacity, the braking distance is the longest, and the temperature rise is the highest.

(6) The forced cooling of the brake has a significant cooling effect than the self-cooling. In 1.5 cycles, the brake temperature has increased by 8.5 °, and there is a tendency for the brake temperature to stabilize.

This result provides new ideas for the research on the development of charging valves with electro-hydraulic closed-loop feedback, the modeling of service brakes for heavy vehicles, static structural parameters, and environme-ntal factors on the output characteristics.

REFERENCES

[1] W. Q. Zhao, "Review and development of wet multiple-disc brakes," *J. Agricult. Machinery*, vol. 33, no. 2, pp. 117–120, Mar. 2002.

[2] D. Qin and D. Sun, "Research on design method of a multiple disc wet brake in lubricated environment," *Chin. J. Mech. Eng.*, vol. 16, no. 4, pp. 391–395, Jul. 2003.

[3] T. H. Luo, F. Y. Li, C. H. Li, X. G. Huang, S. K. Zhu, and Q. G. Hu, "Influence on engagement characteristic of wet brake with considering permeability of paper-base friction materials," *Chin. J. Mech. Eng.*, vol. 35, no. 2, pp. 115–124, Oct. 2014.

[4] B. Tang, J.-L. Mo, Y. K. Wu, X. Quan, M. H. Zhu, and Z. R. Zhou, "Effect of the friction block shape of railway brakes on the vibration and noise under dry and wet conditions," *Tribol. Trans.*, vol. 62, no. 2, pp. 262–273, Mar. 2019.

[5] A. A. Yevtushenko and P. Grzes, "The FEM-modeling of the frictional heating phenomenon in the Pad/Disc tribosystem (A Review)," *Numer. Heat Transf. A, Appl.*, vol. 58, no. 3, pp. 207–226, Aug. 2010.

[6] S. Liu, D. Sun, E. Wu, Y. Luo, and D. Qin, "Application of computerized numerical modeling in multi-state wet wheel hub heat simulations," *Cluster Comput.*, vol. 22, no. S1, pp. 1569–1580, Mar. 2018.

[7] S. K. Singh, H. Abbassi, and P. Tamamidis, "3D investigation into the thermal behavior of the wet multi-disk axle brake of an off-highway machinery," *Appl. Thermal Eng.*, vol. 136, no. 25, pp. 576–588, May 2018.

[8] X. Hu, W. Jiang, B. Guo, J. Zhao, and Z. Luo, "Study on the simulation and test method of static characteristics for series brake valve," *Acta Metrologica Sinica*, vol. 40, no. 6, pp. 1088–1095, Sep. 2019.

[9] W. Yuan and M. Wang, "Design of hydraulic system for mine rubber wheel car based on wet brake," *Saf. Coal Mines*, vol. 50, no. 6, pp. 121–124, Jun. 2019.

[10] M. Gong and H. Wei, "Full power hydraulic brake system based on double pipelines for heavy vehicles," *Chin. J. Mech. Eng.*, vol. 24, no. 5, pp. 790–797, Sep. 2011.

[11] Z. Zhang and B. Liu, "Simulation analysis of the service braking system of fully hydraulic wheeled transporter," *Comput. Simul.*, vol. 32, no. 11, pp. 174–178, Nov. 2015.

[12] J. Chen, X. Liu, T. Wang, X. Gong, H. Sun, G. Wang, and W. Chen, "Charging valve of the full hydraulic braking system," *Adv. Mech. Eng.*, vol. 8, no. 3, pp. 1–11, Feb. 2016.

[13] M. Lin and W. Zhang, "Dynamic simulation and experiment of full power hydraulic brake system," *J. Univ. Sci. Technol. Beijing*, vol. 29, no. 1, pp. 70–75, Jan. 2007.

[14] Z. Yu, W. Han, S. Xu, and L. Xiong, "Review on hydraulic pressure control of electro-hydraulic brake system," *J. Mech. Eng.*, vol. 53, no. 14, pp. 1–15 Jul. 2017.

[15] E. Sabanovic, V. Zuraulis, O. Prentkovskis, and V. Skrickij, "Identification of road-surface type using deep neural networks for friction coefficient estimation," *Sensors*, vol. 20, no. 3, pp. 1–17, Feb. 2020.

[16] J. Cao, C. Song, S. Song, F. Xiao, and S. Peng, "Lane detection algorithm for intelligent vehicles in complex road conditions and dynamic environments," *Sensors*, vol. 19, no. 14, pp. 1–21, Jul. 2019.

[17] B. Moaveni and P. Barkhordari, "Modeling, identification, and controller design for hydraulic anti-slip braking system," *Proc. Inst. Mech. Eng. D, J. Automobile Eng.*, vol. 233, no. 4, pp. 862–876, Mar. 2019.

[18] J. J. Castillo, J. A. Cabrera, A. J. Guerra, and A. Simon, "A novel electrohydraulic brake system with tire–road friction estimation and continuous brake pressure control," *IEEE Trans. Ind. Electron.*, vol. 63, no. 3, pp. 1863–1875, Mar. 2016.

[19] S.-I. Sakai, H. Sado, and Y. Hori, "Dynamic driving/braking force distribution in electric vehicles with independently driven four wheels," *Electr. Eng. Jpn.*, vol. 138, no. 1, pp. 79–89, Jan. 2002.

[20] L. Jin, R. Zhang, B. Tang, and H. Guo, "A fuzzy-PID scheme for low-speed control of a vehicle while going on a downhill road," *Energies*, vol. 13, no. 11, pp. 1–18, Jun. 2020.

[21] A. Klein-Paste, "Airplane braking friction on dry snow, wet snow or slush contaminated runways," *Cold Regions Sci. Technol.*, vol. 150, pp. 70–74, Jun. 2018.

[22] J. Harušinec, A. Suchánek, M. Loulová, and P. Stratovec, "Design of a device to simulate environmental influences on the course of brake tests," in *Proc. MMS*, Sklené Teplice, Slovakia, 2018, pp. 1–9.

[23] L. Henderson and D. Cebon, "Full-scale testing of a novel slip control braking system for heavy vehicles," *Proc. Inst. Mech. Eng. D, J. Automobile Eng.*, vol. 230, no. 9, pp. 1221–1238, Sep. 2015.

[24] H. Pan, X. Guo, X. Pei, and D. Sun, "Pressure controlling of integrated electro-hydraulic braking system with considering driver brake behaviour," *Int. J. Vehicle Des.*, vol. 79, no. 4, pp. 248–272, Nov. 2019.

[25] M. Zamzamzadeh, A. Saifizul, R. Ramli, and M. Soong, "Dynamic simulation of brake pedal force effect on heavy vehicle braking distance under wet road conditions," *Int. J. Automot. Mech. Eng.*, vol. 13, no. 3, pp. 3555–3563, Dec. 2016.

[26] A. A. Sharizli, R. Rahizar, M. R. Karim, and A. A. Saifizul, "New method for distance-based close following safety indicator," *Traffic Injury Prevention*, vol. 16, no. 2, pp. 190–195, Oct. 2014.

[27] M. Zamzamzadeh, A. A. Saifizul, R. Ramli, and M. F. Soong, "Heavy vehicle multi-body dynamic simulations to estimate skidding distance," *Baltic J. Road Bridge Eng.*, vol. 13, no. 1, pp. 23–33, Mar. 2018.

[28] M.-W. Suh, Y.-K. Park, and S.-J. Kwon, "Braking performance simulation for a tractor-semitrailer vehicle with an air brake system," *Proc. Inst. Mech. Eng. D, J. Automobile Eng.*, vol. 216, no. 1, pp. 43–54, Jan. 2002.

[29] J. Zhao, Z. Hu, B. Zhu, and J. Gong, "Integrated model control of brake–wheel system using bond graph method," *Adv. Mech. Eng.*, vol. 10, no. 7, pp. 1–16, May 2018.

YONG YANG received the B.S. degree in mechanical engineering from the Wuhan University of Technology, Wuhan, China, in 2011, and the M.S. degree in mechanical engineering from Guizhou University, Guizhou, China, in 2014. He is currently pursuing the Ph.D. degree in materials science and engineering with the University of Science and Technology Beijing (USTB), Beijing, China.

From 2014 to 2018, he was a Lecturer with Chongqing Three Gorges University, Chongqing, China. His research interests include electromechanical transmission and control systems, fabrication of micro- or nanostructured, and surface functional materials.

HAIBAO WANG was born in Liaoning, China, in 1966. He is currently the Dean, a Professor, and a Master Supervisor with the School of Mechanical Engineering, Chongqing Three Gorges University. Besides, he has published more than 30 academic articles, three works, and more than ten patents in professional journals at home and abroad. His research interests include electromechanical transmission and control, and signal monitoring and processing. He has won the unique honor of Excellent National Teacher and Advanced Federal Individual in education and scientific research.

GUOFENG XIA was born in 1985. He received the Ph.D. degree from the Beijing University of Technology, in 2015. He is currently an Associate Professor and a Master Supervisor with the School of Mechanical Engineering, Chongqing Three Gorges University. He published more than ten SCI/EI articles in the field of mechanical engineering. He also applied for more than 50 patents, including 27 domestic invention patents, three PCT international patents, two U.S. patents, and more than 20 utility model patents. His research interests include precision CNC machining and electronic packaging. He received the Excellent Paper Award of the IEEE International Electronic Packaging Technology Conference (ICEPT-HDP) twice in 2011 and 2012.